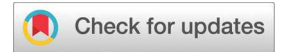
Dalton Transactions



PAPER

View Article Online
View Journal | View Issue



Cite this: *Dalton Trans.*, 2023, **52**, 10942

Received 30th April 2023, Accepted 5th July 2023 DOI: 10.1039/d3dt01292a

rsc li/dalton

Visible light-activatable platinum(IV) prodrugs harnessing CD36 for ovarian cancer therapy†

Amarasooriya M. D. S. Jayawardhana, Srijana Bhandari, Ariela W. Kaspi-Kaneti,‡ Man Kshetri, Zihan Qiu, May Cheline, Hao Shen, Barry D. Dunietz and Yao-Rong Zheng *

We hereby engineered photoactivatable Pt(IV) metallodrugs that harness CD36 to target ovarian cancer cells. Pt(IV) compounds mimic the structure of fatty acids and take advantage of CD36 as a "Trojan horse" to gain entry into the cells. We confirmed that CD36-dependent entry occurs using graphite furnace atomic absorption spectroscopy with ovarian cancer cells expressing different levels of CD36 and a CD36 inhibitor, SSO. Once the Pt(IV) metallodrugs enter the cancer cells, they can be activated to form Pt(III) with characteristics of cisplatin under visible light (490 nm) irradiation, promoting photoinduced electron transfer from the attached fluorophore to the metal center. This light-induced activation can increase the cytotoxicity of the Pt(IV) metallodrugs by up to 20 times toward ovarian cancer cells, inducing DNA damage and enabling efficient elimination of drug-resistant cancer cells.

Introduction

CD36 is an emerging target in cancer therapy due to its significant role in promoting tumor growth, metastasis, and drug resistance. 1-5 As a transmembrane protein that facilitates the uptake of free fatty acids for lipid metabolism, CD36 provides a critical source of energy and membrane components for tumor cells. 1,2,5 Recent evidence suggests that the upregulation of CD36 can fuel tumor growth, metastasis, and drug resistance. 1-3 CD36-based therapies, such as monoclonal antibody and polypeptide treatments, have shown promise in impeding tumor metastasis.3 In ovarian tumors, CD36 is upregulated through its interaction with adipocytes in the tumor microenvironment. Studies have shown that CD36 is upregulated in both primary and metastasized ovarian tumors.^{2,3} Despite these findings, using the upregulation of CD36 to tackle the issue of drug resistance in ovarian cancer remains a long-standing challenge. Conventional platinum-based chemotherapy, the primary treatment for ovarian cancer, often leads to drug resistance.^{6,7} CD36 has been found to be upregulated in drug-resistant ovarian cancer cells, however, there are still

very few studies focusing on addressing this issue through targeting CD36 upregulation.⁸

The approach of using photoactivatable Pt(IV) prodrugs shows promise in the development of novel Pt-based metallodrugs that exhibit high efficacy while minimizing systemic toxicity. 9-17 Compared to cytotoxic Pt(II) payloads, the octahedral Pt(IV) complex is more resistant to ligand substitution. When reduced, the Pt(IV) complex becomes a square-planar Pt(II) center that can be released as the cytotoxic agent if appropriate ligands are chosen. 18 Photoactivation enables the reduction of Pt(IV) complexes to Pt(II) products with light irradiation, which enhances efficacy and reduces systemic toxicity in a spatiotemporally controlled manner. 19-21 Studies have shown that diazido Pt(IV) complexes undergo photo-induced reductive elimination, releasing the cytotoxic Pt(II) products upon UV light irradiation. 19,22-24 Additionally, flavin adenine dinucleotide has been demonstrated to act as a photocatalyst, converting Pt(IV) to cisplatin upon irradiation at 460 nm.20 Moreover, recent research by Zhu has reported a series of novel carboplatin/oxaliplatin-based Pt(w) prodrugs that can be activated by visible light. 21,25-27 Despite these developments, studies of visible light-activatable Pt(w) prodrugs remain limited.

This article describes the development of the first Pt(IV) prodrug (compound 1 in Fig. 1) that can be activated by visible light and exploits the CD36-dependent cell entry mechanism to enhance efficacy against drug-resistant ovarian cancer cells. Previous studies have demonstrated that lipophilic Pt(IV) prodrugs with hydrocarbon tails possess high potency and promising pharmacokinetics. Our recent research has also shown that such prodrugs can utilize CD36 upregulation to

Department of Chemistry and Biochemistry, Kent State University, Kent, OH 44242, USA. E-mail: yzheng7@kent.edu

‡Current: Department of Chemistry, University of La Verne, 1950 3rd Street, La Verne, CA 91750, USA.

[†]Electronic supplementary information (ESI) available: Experimental data regarding the synthesis and characterization of 1 and the corresponding computational studies, cellular uptake, and flow cytometry analysis. See DOI: https://doi.org/10.1039/d3dt01292a

I. CD36-dependent cell entry

Extracellular

II. Light-triggered cellular responses

Nuclear DNA

Cell

Dalton Transactions

Fig. 1 Graphical representation of the mechanism of action of the visible light-activatable Pt(w) prodrug (1).

Photoactivation

Damage

effectively target ovarian cancer cells.⁸ In this new project, we have modified the Pt(IV) prodrug by attaching a fluorescein moiety, which enables photoactivation upon 490 nm irradiation. By combining CD36-dependent cell entry and photoactivation, the fluorescein–Pt(IV) conjugate shows excellent efficacy in eliminating ovarian cancer cells in a controlled manner. We also provide computational analysis of the optical properties of the complex.

Results and discussion

Synthesis and characterization of the photoactivatable Pt(v) prodrug (1)

The synthesis of the Pt(IV) prodrug (1) is depicted in the ESI.† Firstly, the fatty acid-like Pt(IV) prodrug (C16Pt) was synthesized using a reported procedure.8 Next, it was conjugated with fluorescein thiocarbamylethylenediamine via the HATUcatalyzed amide bond formation reaction. The overall yield was 80.7%. The fluorescein-conjugated Pt(IV) compound (1) was characterized using ¹H and ¹³C NMR spectroscopy, electrospray ionization mass spectrometry (ESI-MS), and HPLC. The broad signal at 6.5 ppm in the ¹H NMR spectrum (Fig S1B in the ESI†) corresponds to the amine groups of the Pt(IV) center and fluorescein, while the signals at 0.85 ppm and 1.20 ppm are from the C16 tail attached to the carbamate. The isotopically resolved signal at m/z = 1133.3343 in the ESI-MS spectrum (Fig S1D†) agrees with the theoretical value of 1 (m/z =1133.3340). HPLC analysis of the final product indicated a purity of 96% using the described synthetic method.

CD36-dependent cell entry of the Pt(IV) prodrug (1)

We conducted further experiments to investigate the ability of the Pt(IV) prodrug (1) to harness CD36 for facilitating its entry

into drug-resistant ovarian cancer cells. Specifically, we evaluated the CD36-dependent cell entry of compound 1 by using both a cisplatin-sensitive ovarian cancer cell line (A2780) and its cisplatin-resistant counterpart (A2780cis). We performed western blot analysis to assess the expression of CD36 in both cell lines. As shown in Fig. 2A, CD36 was found to be expressed in A2780cis cells, but not in A2780 cells, which is consistent with our previous findings.8 Based on this, we hypothesized that the upregulation of CD36 could facilitate the cell entry of 1. We then used graphite furnace atomic absorption spectroscopy (GFAAS) to measure the cellular uptake of 1 in both cell lines. The results showed that 1 preferentially accumulated in A2780cis cells (179 ± 5 pmol Pt per μg proteins) compared to A2780 cells (77.4 \pm 1.4 pmol Pt per μ g proteins), but cisplatin did not exhibit any significant difference in intracellular accumulation across these cell lines. Furthermore, we used Sulfo-N-succinimidyl oleate (SSO) to inhibit CD36-dependent cell entry of compound 1. SSO is a fatty acid-like small molecule that blocks CD36-dependent cell entry by covalently binding to the protein. As shown in Fig S2 in the ESI,† the preferential uptake of 1 in A2780cis cells was considerably hampered by pre-treatment with SSO. However, despite the inhibition by SSO, the high lipophilicity of 1 allowed its superior uptake compared to that of cisplatin.

Photoactivation of the Pt(w) prodrug (1)

In the next step, we evaluated the photoactivation of the Pt(IV) prodrug (1) and its light-triggered cellular responses *in vitro*. We hypothesized that the photoactivation of 1 leads to the release of a fluorescein derivative (2) and cisplatin, as shown in Fig. 3A. To validate our hypothesis, we used fluorescence spectroscopy, cellular imaging, and flow cytometry. Upon 20-minute exposure to 490 nm light (2.36 mW cm⁻²), we observed fluorescence turn-on in 1 due to the cleavage of the fluorescein derivative from the heavy metal center, as depicted in Fig. 3B. In addition, we verified the fluorescence turn-on phenomenon in live cells that were treated with Pt(IV) prodrug 1 and exposed to 490 nm irradiation, as demonstrated in Fig. 3C. Next, we utilized flow cytometry to investigate the extent of nuclear DNA damage by analyzing the extent of phos-

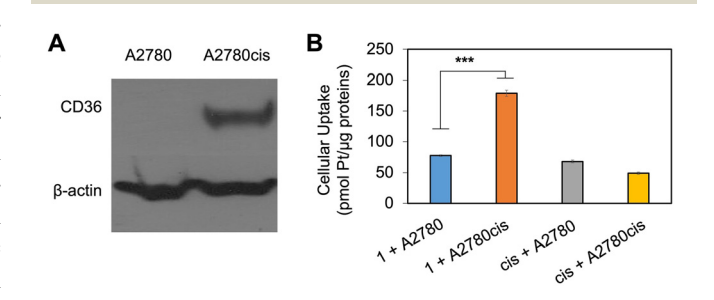


Fig. 2 CD36-dependent cellular entry and cytotoxicity profiles of the visible light-activatable Pt(IV) prodrug (1): (A) western blot analysis of CD36 expression in A2780 and A2780cis ovarian cancer cells and (B) GFAAS measurement of cellular uptake of 1 and cisplatin (cis) against A2780 (left) and A2780cis (right) cells (10 μ M, 4 h). ***P < 0.0005 by the t test (n = 3, mean \pm SEM).

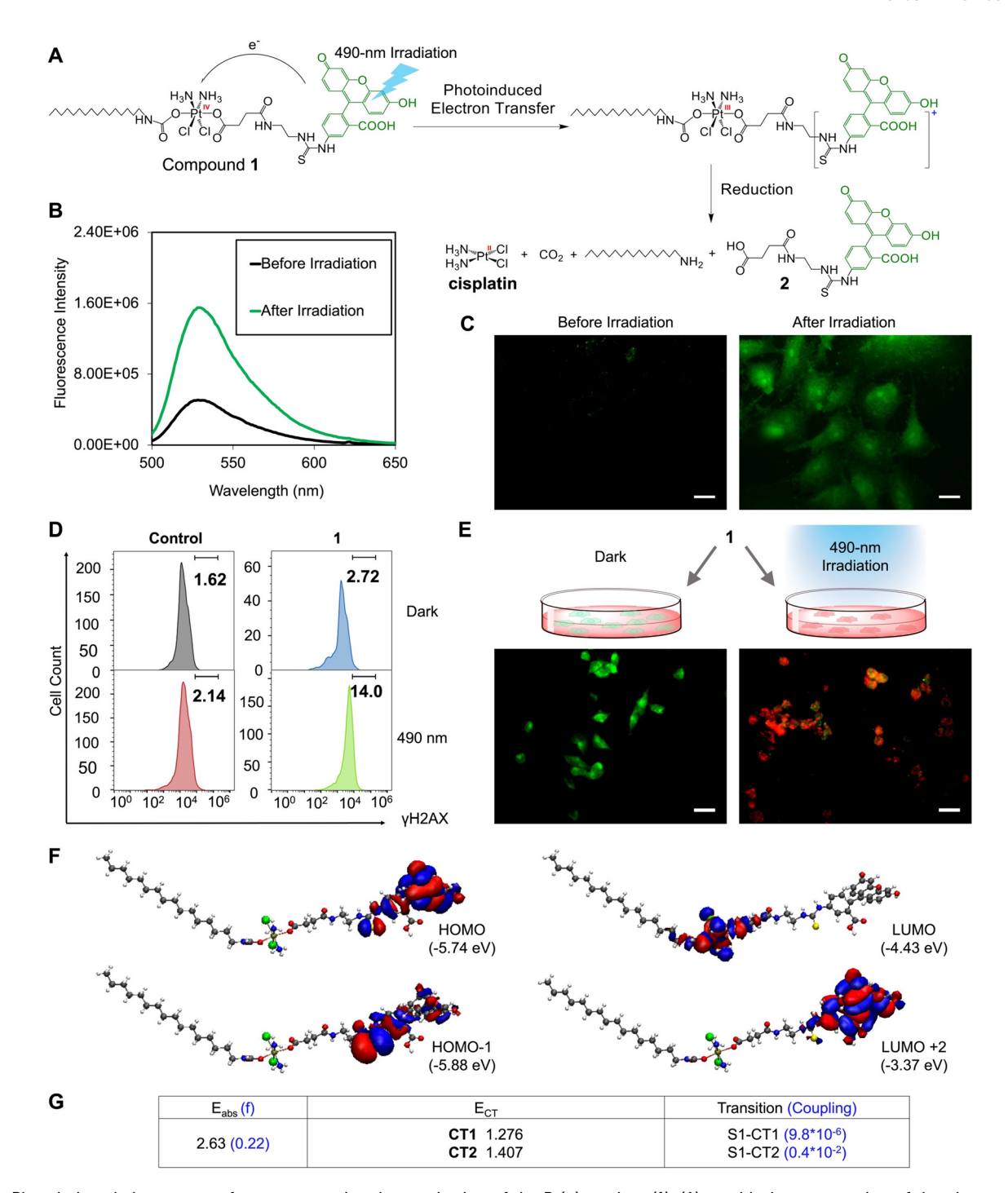


Fig. 3 Photoinduced electron transfer empowers the photoactivation of the Pt(|v|) prodrug (1): (A) graphical representation of the photoactivation process: 490 nm irradiation facilitates photoinduced electron transfer from the fluorescein dye to the Pt(|v|) center, leading to the formation of the Pt (|v|) intermediate. This intermediate is rapidly reduced to release the axial ligands and the Pt(|v|) species, triggering subsequent cellular responses, including nuclear DNA damage and cell death; (B) fluorescence spectra of compound 1 in PBS recorded before and after 20 min irradiation of 490 nm light (2.36 mW cm⁻²); (C) fluorescence images of the 1-treated A549 cells (10 μ M, 6 h) recorded before and after 20 min irradiation of 490 nm light; (D) Flow cytometry analysis of nuclear DNA damage of the A2780cis cells without (left, **control**) and with the treatment of 1 (right, 10 μ M, 6 h) in the absence (dark) or presence (490 nm) of 20 min irradiation by 490 nm light (2.36 mW cm⁻²); (E) fluorescence images of the live (green)/dead (red) assays of the A2780cis cells treated with 1 ([Pt] = 20 μ M, 6 h) recorded without (left) or with (right) 490 nm irradiation. Scale bar is 20 μ m; (F) electronic distributions of the HOMO-1, HOMO, LUMO, and LUMO+2 of 1; and (G) electronic excited state energies and the oscillator strength of the absorbing state (S1), electronic coupling of S1 with the CT states.

phorylation of H2AX (yH2AX), a known biomarker of DNA damage, since cisplatin is known to target nuclear DNA. Our results demonstrated that treatment with the Pt(IV) prodrug (1) with 490 nm irradiation resulted in a significant increase in γH2AX, indicating light-triggered nuclear DNA damage, as shown in Fig. 3D. In contrast, treatment with 1 alone in the dark did not cause significant nuclear damage, suggesting that most of the Pt payloads were not activated without light. We further employed cellular imaging studies and flow cytometry analysis to confirm that light-triggered nuclear DNA damage ultimately resulted in cell death. As demonstrated by the LIVE/DEAD cell assay results in Fig. 3E, the treatment with 1 (20 µM, 6 h) and 490 nm irradiation induced cell death in A2780cis cells. In contrast, the cells treated with 1 in the dark did not show cell death. Flow cytometry analysis (Fig. S3†) further confirmed that a large population of the 1-treated cells underwent cell death in response to light irradiation. Therefore, the photoactivation of the Pt(IV) prodrug is found to release cisplatin payloads, which induces light-triggered nuclear damage and subsequent cell death.

Dalton Transactions

Computational analysis of the photoactivation process

We investigated the photoactivation of the prodrug (1). In Fig. 3A we illustrate the proposed mechanism, where photoexcitation of the fluorescein dye with 490 nm visible light induces electron transfer to the Pt(IV) center, forming a Pt(III) intermediate. This intermediate is rapidly reduced to the Pt(II) species. Our calculations resolve the relevant excited states of 1 to the photoinduced electron transfer step.24,25 In the Pt complex, the calculated excitation energy of the absorbing state is 2.63 eV (oscillator strength [OS] of 0.22, mostly involving the replacement of the highest occupied molecular orbital (HOMO) by the lowest unoccupied molecular orbital (LUMO+2), which is red shifted compared to 2.89 eV (OS of 0.51) for free fluorescein and is in good agreement with the measured value of 2.53 eV (equivalent to 490 nm). The two lowest CT states, CT1 of 1.28 eV and CT2 of 1.41 eV, involve electron transfer from the fluorescein (donor) to the Pt(IV) center (acceptor). The CT1 and CT2 states are dominated by the replacement of the HOMO and HOMO-1, respectively, by LUMO (see Fig. 3F for an illustration of the orbitals). Both HOMO and HOMO-1 are localized in the fluorescein moiety, whereas the LUMO is localized towards the Pt(IV) center. Fig. 3G lists the excitation energies of the S1 and CT states and the S1 to CT coupling energies. The CT process involving the CT2 state is indicated to dominate the reduction process leading to Pt(III). The coupling between the absorbing state to CT2 is 4.0×10^{-3} eV, while that to CT1 is significantly smaller, effectively vanishing at 9.8×10^{-6} eV. Overall, these results support the assertion that electron transfer follows photoexcitation to affect the reduction of the Pt(IV) prodrug.

Cytotoxicity profiles of the Pt(IV) prodrug (1)

Our primary objective was to evaluate the cytotoxicity of 1 and establish its correlation with CD36 expression and light exposure. To determine the viability of cells with varying levels

of CD36 that were treated with 1 and light irradiation, we used 3-(4,5-dimethylthiazol-2-yl)-2,5-diphenyltetrazolium (MTT) assays. The IC50 values, which indicate the concentration required to inhibit growth by 50%, are illustrated in Fig. 4A. In the absence of 490 nm irradiation (dark), 1 exhibits a similar cytotoxicity profile as cisplatin. Notably, upon irradiation, the IC_{50} values of 1 were decreased to 8.40 \pm $0.50 \mu M$ in A2780 and $8.55 \pm 0.80 \mu M$ in A2780cis, which is up to 20 times more potent compared to cisplatin. In the absence of light, most of the payloads are not in the active form. So, even though the cellular uptake of 1 excels that of cisplatin, 1 still has low potency. In the dark, 1 demonstrates significantly lower cytotoxicity compared to C16Pt. Once light irradiation is applied, the payloads are activated, resulting in a much higher potency, surpassing that of C16Pt. Accordingly, we calculated the photocytotoxicity indices (PI) of 1 based on IC50(light)/ $IC_{50}(dark)$ as shown in Fig. 4A. Interestingly, 1 exhibits a much higher PI (19.3) against A2780cis compared to A2780 (7.5). This is consistent with the CD36-dependent uptake described above. The upregulated CD36 in A2780cis facilitates payload accumulation, which is twice that in A2780. In sum, these results support that the photoactivatable Pt(IV) prodrug (1) harnesses CD36 to facilitate their cell entry for killing A2780cis cisplatin-resistant CD36-overexpressing ovarian cancer cells in a light-controlled manner.

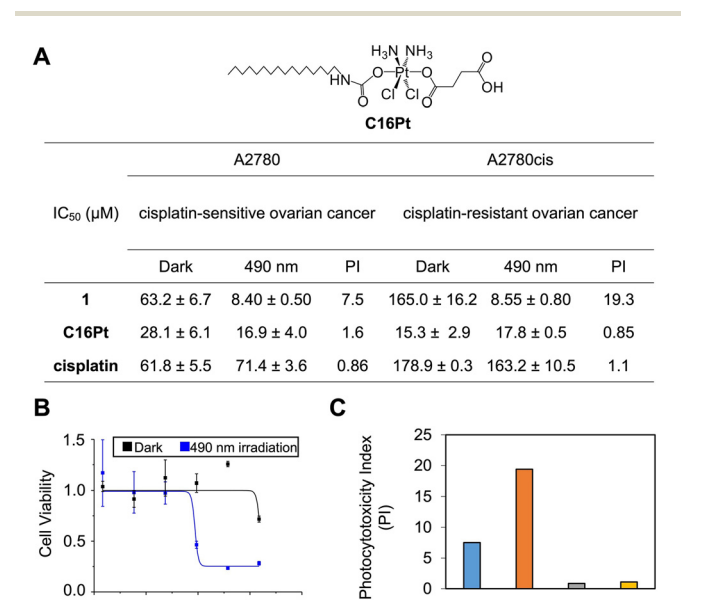


Fig. 4 Cytotoxicity profiles of the visible light-activatable Pt(IV) prodrug (1): (A) the table of IC_{50} values and the photocytotoxicity index (PI) determined by MTT assays for 1, C16Pt, and cisplatin against A2780 and A2780cis with 24 h incubation in the absence (dark) or presence (490 nm) of 20 min irradiation by 490 nm light (2.36 mW cm $^{-2}$); (B) representative killing curves of 1 against A2780cis cells; and (C) bar graph of the photocytotoxicity indices (PI) of 1 and cisplatin against A2780 and A2780cis cells.

0

2

Log[Pt Conc. (µM)

cis* A2780

ois * A2780cis

1 * A2780cis

Paper Dalton Transactions

Conclusions

In conclusion, we have presented a novel chemical design for Pt(iv) prodrugs that are activated by visible light and exploit the upregulated CD36 to enhance cellular uptake in ovarian cancer. In this design, the fluorescein axial ligand captures 490 nm photon flux and induces photoinduced electron transfer for the reduction (or activation) of the Pt(IV) prodrugs, leading to light-induced cellular responses such as nuclear DNA damage and cell death. Notably, the other lipophilic axial ligand of the Pt(IV) centers promotes CD36-dependent cell entry, making it effective against CD36-upregulated cisplatinresistant ovarian cancer cells. This work represents a proof-ofconcept study towards developing tumor-specific photoactivatable metallodrugs. The photoactivation mechanism may mitigate off-target effects resulting from CD36 expression in normal tissues, making it a promising approach for future translational applications.

Experimental

General information

All reagents were purchased from Strem, Sigma Aldrich or Alfa Aesar and used without further purification. Fluorescein thiocarbamylethylenediamine was synthesized according to the reported literature.³⁷ All reactions were carried out under normal atmospheric conditions. A Bruker 400 NMR spectrometer was used for NMR data acquisition (frequency: 400 MHz for ¹H NMR; 100 MHz for ¹³C NMR) and the plots were generated using TOPSPIN 3.2 software. Chemical shifts in ¹H and ¹³C NMR spectra were internally referenced to solvent signals (¹H NMR: DMSO at δ = 2.50 ppm; ¹³C NMR: DMSO at δ = 39.51 ppm). The high-resolution mass spectra of generated ions were recorded on an Exactive Plus mass spectrometer (Thermo Scientific, Bremen, Germany). The blue LED light source is a Kessil A160WE LED. The photon flux at 490 nm was determined using a Thorlabs optical power meter, and it is 2.36 mW cm⁻². GFAAS measurements were taken on a PerkinElmer PinAAcle 900Z spectrometer. The Pt concentrations for all the studies have been quantified using GFAAS. Elemental analysis was performed on a TruSpec Micro, CHNS analyzer from LECO Corporation. Fluorescence spectra were recorded on FluoroMax-3 fluorescence spectrophotometer using the software called FluorEssence. Fluorescence images were acquired using an Olympus IX70 inverted epifluorescence microscope equipped with a digital CCD camera (QImaging). Images were processed and intensities were quantified using ImageJ software (NIH). Flow cytometry was carried out on a FACSAriaTMII flow cytometer. The Live/Dead cell assay was carried out using the Invitrogen (Thermo Fisher Scientific) LIVE/DEADTM Cell Viability Kit (Cat. No. L3224).

Synthesis of compound 1

To a mixture of C16Pt (39.2 mg, 0.056 mmol) and HATU (21.3 mg, 0.056 mmol) was added 1 mL of anhydrous DMF.

The solution was stirred for 20 min at r.t. Then, to the reaction mixture, 0.4 mL anhydrous DMF solution of fluorescein thiocarbamylethylenediamine (30 mg, 0.067 mmol) was added. After 30 min of stirring at r.t., DIPEA (19 µL, 0.112 mmol) was added. The vial was covered with aluminum foil, and the reaction mixture was stirred for 6 h at r.t. A total of 4 mL brine was added to the reaction mixture to precipitate the product. Then, the precipitate was collected by centrifugation, and washed with excess water. The final product was obtained after lyophilization. Yield: 52.0 mg (80.7%). ¹H NMR (400 M Hz, DMSO-d₆): δ : 0.852 (NHCH2(CH2)14CH₃, t, J = 6.8 Hz, 3H), 1.232 (NHCH2(CH2)14CH₃, m, 28H), 2.247-2.477 (COCH2CH2CO, m, 4H), 2.740-2.838 (NHCH2CH2NH-FITC, m, 4H), 3.207-3.275 (NHCH2(CH2)14CH3, m, 2H), 6.505-6.672 (NH3, NHCH2(CH2)14CH₃, FITC, m, 13H), 7.176 (FITC, d, J =8.4 Hz, 1H), 7.809 (FITC, s, 1H), 7.964 (NHCH2CH2NH-FITC, t, J = 5.6 Hz, 2H), 8.223 (FITC, s, 2H); ¹³C NMR (100 MHz, DMSO-d₆): δ: 180.3, 174.3, 172.8, 172.0, 169.0, 164.4, 160.0, 152.3, 129.5, 113.0, 110.2, 102.7, 41.5, 38.8, 37.5, 31.9, 31.7, 30.5, 30.4, 29.5, 29.4, 29.3, 29.2, 26.9, 26.2, 22.5, 14.4. Anal. Calcd for $C_{44}H_{62}Cl_2N_6O_{10}PtS\cdot(H_2O)_3$: C, 44.52; H, 5.77; N, 7.08. Found: C, 44.29; H, 5.52; N, 7.17. HR-MS (positive mode) for $[C_{44}H_{62}Cl_2N_6O_{10}PtS + H]^+$: m/z calc: 1133.3340, m/z obsd: 1133.3343; purity: 96% determined by HPLC.

Western blotting experiments for CD36 expression in A2780 and A2780cis cell lines

A2780 and A2780cis cells were collected and lysed using RIPA buffer. 2× loading dye was added to the protein samples. The samples were heated at 100 °C for 7-10 min, and quickly centrifuged. Meanwhile, gel electrophoresis equipment was set up, and 1× running buffer was filled in the tank. The denatured protein samples were injected into the SDS-PAGE gel, 20 µg per well. The gel was run at 200 V for 38 min and transferred to a sandwich structure model to be prepared for gel transfer, which used a PVDF membrane to catch the proteins. The gel transfer took 90 min at 28 V by wet transfer. The PVDF membrane was cut based on the MW of the proteins (CD36 85-90 kDa and β-actin 45 kDa). The membrane was placed in block buffer and gently shaken at r.t. for 1 h. The membrane was incubated with the primary antibodies CD36 (BioLegend®, San Diego, CA, USA) and β-actin overnight at 4 °C with gentle shaking. The membrane was washed with 1× TBST 3 times at R.T., and 10 min each with gentle shaking. The membrane was incubated with the secondary antibody at r.t. for 1 h with gentle shaking. The membrane was washed with 1× TBST 3 times again at r.t., 10 min each with gentle shaking. The ECL substrate was applied to the membrane. A western blotting (WB) film was used to cover the membrane and pressed for a few seconds in a dark room, and an X-ray film processor was used to detect and analyse the chemiluminescence signal of WB.

GFAAS analysis of cellular Pt contents of A2780 and A2780cis cells

A2780 and A2780cis cells were seeded in a 6-well plate at a concentration of 2×10^5 cells per well and incubated at 37 °C,

under 5% CO₂ overnight. These cells were treated with cisplatin or compound 1 ([Pt] = 10 μM) for 4 h at 37 °C, under 5% CO₂. The remaining live cells were harvested by trypsinization and counted. The cells were then digested in 200 μL 65% HNO₃ at r.t. overnight. The Pt contents in the cells were analyzed by GFAAS. All experiments were performed in triplicate.

GFAAS analysis of cellular Pt contents of A2780cis cells treated with SSO

A2780cis cells were seeded in a 6-well plate at a concentration of 2×10^5 cells per well and incubated at 37 °C, under 5% CO $_2$ overnight. The cells were treated with 200 μM sulfo-N-succinimidyl oleate (SSO, Cayman Chemical Company, Michigan, USA) in the RPMI medium without FBS and PS to avoid the fatty acid present in FBS, and incubated for 30 min at 37 °C, under 5% CO $_2$. Then, the RPMI medium was removed and the fresh complete RPMI medium was added to the wells. Compound 1 or cisplatin (10 μM) was added into cells and incubated for 4 h at 37 °C, under 5% CO $_2$. The Pt contents in the cells were analyzed by GFAAS following the abovementioned procedure.

Fluorescence spectra of compound 1 with and without 20 min irradiation with 490 nm light

 $80~\mu M$ solution of compound 1 was prepared in PBS (Phosphate Buffer Saline) at r.t. Fluorescence emission spectra were recorded on a FluoroMax-3 fluorescence spectrophotometer in a 500–650 nm range with excitation at 490 nm. Next, the solution was irradiated with a 490 nm LED for 20 min and spectra were recorded again.

Fluorescence imaging experiments for A549 cells treated with compound 1 with and without 20 min irradiation with 490 nm light

A549 cells were seeded in two imaging disks (MatTek) at a concentration of 5 \times 10 4 cells with 2 mL of complete medium and incubated for 24 h at 37 °C. The cells in both disks were then treated with compound 1 (10 $\mu M)$ and incubated for 6 h at 37 °C, under 5% CO2. Next, one disk was irradiated with a 490 nm LED for 20 minutes. Both disks were washed 3 times with 1 mL of PBS and images were acquired using an Olympus IX70 inverted epifluorescence microscope equipped with a digital CCD camera (QImaging). Images were processed and intensities were quantified using ImageJ software (NIH).

Flow cytometry analysis of nuclear damage using γH2AX

A2780cis cells were seeded in 3 wells of two 6-well plates at a concentration of 2×10^5 cells per well and incubated for 24 h at 37 °C, under 5% CO_2 . Next, the cells were treated with cisplatin or compound 1 (10 μ M) while the third well was kept as a control. Cells were then incubated for 6 h at 37 °C, under 5% CO_2 . After 6 h, one well plate was irradiated with 490 nm LED for 20 minutes. Both well plates were washed with the fresh medium and filled with 5 mL of the fresh medium. Plates were then incubated for 24 h at 37 °C, under 5% CO_2 . Next, the live cells were collected and washed with 1 mL PBS. 250 μ L of BD

permeabilization solution was added to re-suspend the cells and incubated for 20 min at 4 $^{\circ}$ C. The cell pellet was collected and washed twice with 1 mL of 1× washing buffer. To the pellet with 50 μ L of buffer, 5 μ L Alexa Fluor 647-anti H2AX antibody solution was added and incubated in the dark for 60 min at r.t., centrifuged (1400 rpm, 5 min) and the cell pellet was suspended in 300 μ L of PBS and analyzed using a flow cytometry APC channel on a FACSAriaTMII flow cytometer (BD Biosciences, Franklin Lakes, NJ, USA).

Flow cytometry analysis of cell death using propidium iodide (PI)

A2780cis cells were seeded in 3 wells of two 6-well plates at a concentration of 2×10^5 cells per well and incubated for 24 h at 37 °C. Next, the cells were treated with cisplatin or compound 1 (20 μ M) while the third well was kept as a control. Cells were then incubated for 6 h at 37 °C. After 6 h, one well plate was irradiated with 490 nm LED for 20 minutes. Both well plates were washed with the fresh medium and filled with 5 mL of the fresh medium. Plates were then incubated for 24 h at 37 °C. Next, the medium was collected in clean 15 mL falcon tubes along with washed PBS solution. 1 mL trypsin was added to the wells. After 5 min, cell suspensions were transferred to the falcon tubes that contained the medium and PBS and centrifuged at 400-500g at 4 °C for 5 min. The cell pellet was re-suspended in 1 mL PBS and the cells were counted. The cell pellet was collected again and an appropriate amount of 1x binding buffer was added to reach a concentration of 10⁶ cells per mL. 100-µL cell suspensions were added to new 2 mL Eppendorf tubes and 5 µL of PI solution was added. Cells were gently vortexed and incubated at r.t. for 15 min in the dark. 400-μL of 1× binding buffer was added to each Eppendorf tube and the cell suspensions were transferred to flow cytometry tubes. Flow cytometry analysis was carried out using the PerCP/Cy5.5 channel on a FACSAria™II flow cytometer (BD Biosciences, Franklin Lakes, NJ, USA).

LIVE/DEAD cell viability assays

A2780cis cells were cultured in two imaging disks (MatTek) at a concentration of 5×10^4 cells with 2 mL of the complete medium and incubated for 24 h at 37 °C. The cells in both disks were then treated with compound 1 (20 µM) and incubated for 6 h at 37 °C, under 5% CO₂. Next, one disk was irradiated with a 490 nm LED for 20 minutes. Media in both disks were replaced with the fresh RPMI complete medium and incubated overnight. Before the assay, the cells were washed with 1 mL PBS and 1 mL dye-free RPMI to remove serum esterase activity generally present in serum-supplemented growth media. A 500 µL volume of LIVE/DEAD working solution (formed by mixing 2 µM calcein AM and 2 µM ethidium homodimer-1 in PBS) was carefully added to the disks, which were then incubated at r.t. for 30 min. Images were acquired using an Olympus IX70 inverted epifluorescence microscope equipped with a digital CCD camera (QImaging). Images were processed and intensities were quantified using ImageJ software (NIH).

Paper Dalton Transactions

Computational methods

Fluorescein and compound 1 are optimized in their ground state using density functional theory (DFT) at the B3LYP/6-31G* level for O, N, C, H, Cl and S atoms and LANL2DZ effective core potential for the Pt atom, in PCM representing water as the solvent. All the excited state calculations were performed using time dependent DFT (TDDFT) with screened range separated hybrid (SRSH) based on the PBE functional with PCM.38,39 The SRSH-PCM is a recently developed framework that is based on a polarization consistent framework between the functional parameters determining the weight of the exact exchange at long range and the reaction field implementing the PCM, where the same dielectric constant is invoked. The optimally tuned parameter for fluorescein was tuned following the 12 scheme and was found to be 0.148 bohr⁻¹ in the gas phase, where the beta parameter is reset according to the dielectric constant.³⁸ The same tuned value was used for the complex. All calculations were performed using Q-Chem v5.40 Electronic state coupling energies are calculated using fragment charge differences [jcp, 177, 5607].

MTT assays of cisplatin, C16Pt, and 1 against A2780 and A2780cis cells with and without 20 min irradiation with 490 nm light

The cells (A2780 and A2780cis) were seeded in 96-well microplates (two plates from each cell line) in 100 µL cell suspensions (2 \times 10⁴ cells per mL) per well to begin with and were incubated for 24 h at 37 °C under 5% CO2. Next, a 50 µL volume of RPMI with various concentrations of Pt compounds was added to each well of the microplates. The cells were then incubated for an additional 6 h at 37 °C, under 5% CO2. Next, one plate was kept in the dark and other the plate was irradiated with 490 nm LED for 20 minutes. After irradiation, the medium in both plates was aspirated and filled with 150 μL of the fresh medium followed by one time washing with 200 µL of the fresh medium. The plates were then incubated for 24 h at 37 °C, under 5% CO2. Next, a volume of 30 µL MTT (Alfa Aesar) (5 mg mL⁻¹ in PBS) was added to the cells and then the cells were incubated for an additional 2-4 h at 37 °C, under 5% CO₂. The solutions were then aspirated, leaving behind insoluble purple formazan. A volume of 200 µL DMSO was added to the wells and the plates were shaken for 10 min. Next, the microplates were analyzed for absorbance at 562 nm with an ELx800 absorbance reader (BioTek, Winooski, VT, USA). Finally, the data were analyzed using Origin software to produce dose-response curves and to determine IC50 values. All experiments were performed in triplicate.

Conflicts of interest

There are no conflicts to declare.

Acknowledgements

Y.-R. Z. acknowledges the financial support provided by the R15 grant (1R15CA249712-01A1) provided by the National Cancer Institute and the Farris Family Innovation Fellowship and LaunchPad Award provided by Kent State University. Y.-R. Z. acknowledges the support from the Research Council of Kent State University. B. D. D. acknowledges support from the Department of Energy, Basic Energy Sciences grant no. DE-SC0016501 and Kent State University for partial support and for generous resource allocation at the Ohio Supercomputer Center (project PAA-0213). A. M. D. S. J. acknowledges the financial support provided by the Healthy Communities Research Institute at Kent State University.

References

- 1 G. Pascual, A. Avgustinova, S. Mejetta, M. Martin, A. Castellanos, C. Attolini, A. Berenguer, N. Prats, A. Toll, J. Hueto, C. Bescos, L. Di Croce and S. Benitah, *Nature*, 2017, 541, 41.
- A. Ladanyi, A. Mukherjee, H. Kenny, A. Johnson, A. Mitra,
 S. Sundaresan, K. Nieman, G. Pascual, S. Benitah,
 A. Montag, S. Yamada, N. Abumrad and E. Lengyel,
 Oncogene, 2018, 37, 2285–2301.
- 3 S. Wang, A. Blois, T. El Rayes, J. Liu, M. Hirsch, K. Gravdal, S. Palakurthi, D. Bielenberg, L. Akslen, R. Drapkin, V. Mittal and R. Watnick, *Sci. Transl. Med.*, 2016, 8, 329ra34.
- 4 W. W. Feng, O. Wilkins, S. Bang, M. Ung, J. Li, J. An, C. Del Genio, K. Canfield, J. DiRenzo, W. Wells, A. Gaur, R. B. Robey, J. Y. Guo, R. L. Powles, C. Sotiriou, L. Pusztai, M. Febbraio, C. Cheng, W. B. Kinlaw and M. Kurokawa, Cell Rep., 2019, 29, 3405–3420.
- 5 M. J. Watt, A. K. Clark, L. A. Selth, V. R. Haynes, N. Lister, R. Rebello, L. H. Porter, B. Niranjan, S. T. Whitby, J. Lo, C. Huang, R. B. Schittenhelm, K. E. Anderson, L. Furic, P. R. Wijayaratne, M. Matzaris, M. K. Montgomery, M. Papargiris, S. Norden, M. Febbraio, G. P. Risbridger, M. Frydenberg, D. K. Nomura and R. A. Taylor, *Sci. Transl. Med.*, 2019, 11, eaau5758.
- 6 D. Wang and S. J. Lippard, Nat. Rev. Drug Discovery, 2005, 4, 307–320.
- 7 D. Holmes, Nature, 2015, 527, S218-S219.
- 8 A. M. D. S. Jayawardhana, M. Stilgenbauer, P. Datta, Z. Qiu, S. Mckenzie, H. Wang, D. Bowers, M. Kurokawa and Y. R. Zheng, *Chem. Commun.*, 2020, **56**, 10706–10709.
- 9 M. D. Hall and T. W. Hambley, *Coord. Chem. Rev.*, 2002, 232, 49–67.
- 10 E. Wexselblatt and D. Gibson, *J. Inorg. Biochem.*, 2012, **117**, 220–229.
- 11 Z. Dai and Z. Wang, Molecules, 2020, 25, 5167.
- 12 H. Lu, S. He, Q. Zhang, X. Li, Z. Xie, Z. Wang, Y. Qi and Y. Huang, *Biomater. Sci.*, 2021, 9, 7115–7123.

- 13 M. Imran, W. Ayub, I. S. Butler and R. Ziaur, *Coord. Chem. Rev.*, 2018, 376, 405–429.
- 14 K. Mitra, C. E. Lyons and M. C. T. Hartman, *Angew. Chem., Int. Ed.*, 2018, 57, 10263–10267.
- 15 J. A. Roque III, H. D. Cole, P. C. Barrett, L. M. Lifshits, R. O. Hodges, S. Kim, G. Deep, A. Francés-Monerris, M. E. Alberto, C. G. Cameron and S. A. McFarland, *J. Am. Chem. Soc.*, 2022, 144, 8317–8336.
- 16 A. Mani, T. Feng, A. Gandioso, R. Vinck, A. Notaro, L. Gourdon, P. Burckel, B. Saubaméa, O. Blacque, K. Cariou, J.-E. Belgaied, H. Chao and G. Gasser, *Angew. Chem.*, *Int. Ed.*, 2023, e202218347.
- 17 D. Havrylyuk, A. C. Hachey, A. Fenton, D. K. Heidary and E. C. Glazer, *Nat. Commun.*, 2022, **13**, 3636.
- 18 A. W. Kaspi-Kaneti, S. Bhandari, A. Schubert, S. D. Huang and B. D. Dunietz, *ChemPhysChem*, 2021, 22, 106–111.
- 19 F. S. Mackay, J. A. Woods, P. Heringová, J. Kaspárková, A. M. Pizarro, S. A. Moggach, S. Parsons, V. Brabec and P. J. Sadler, *Proc. Natl. Acad. Sci. U. S. A.*, 2007, 104, 20743– 20748.
- 20 M. Martinez-Calvo and J. Mascarenas, *Coord. Chem. Rev.*, 2018, **359**, 57–79.
- 21 Z. Wang, N. Wang, S.-C. Cheng, K. Xu, Z. Deng, S. Chen, Z. Xu, K. Xie, M.-K. Tse, P. Shi, H. Hirao, C.-C. Ko and G. Zhu, *Chem*, 2019, 5, 3151–3165.
- 22 C. Imberti, P. Zhang, H. Huang and P. J. Sadler, *Angew. Chem.*, *Int. Ed.*, 2020, 59, 61–73.
- 23 H. Shi, I. Romero-Canelón, M. Hreusova, O. Novakova, V. Venkatesh, A. Habtemariam, G. J. Clarkson, J. I. Song, V. Brabec and P. J. Sadler, *Inorg. Chem.*, 2018, 57, 14409– 14420.
- 24 N. J. Farrer, L. Salassa and P. J. Sadler, *Dalton Trans.*, 2009, 10690–10701.
- 25 Z. Deng, N. Wang, Y. Liu, Z. Xu, Z. Wang, T. C. Lau and G. Zhu, J. Am. Chem. Soc., 2020, 142, 7803–7812.
- 26 H. Yao, S. Chen, Z. Deng, M. K. Tse, Y. Matsuda and G. Zhu, *Inorg. Chem.*, 2020, 59, 11823–11833.
- 27 Z. Deng, C. Li, S. Chen, Q. Zhou, Z. Xu, Z. Wang, H. Yao, H. Hirao and G. Zhu, *Chem. Sci.*, 2021, **12**, 6536–6542.
- 28 Y.-R. Zheng, K. Suntharalingam, T. C. Johnstone, H. Yoo, W. Lin, J. G. Brooks and S. J. Lippard, *J. Am. Chem. Soc.*, 2014, 136, 8790–8798.
- 29 M. Miller, Y. Zheng, G. Suresh, C. Pfirschke, H. Zope, C. Engblom, R. Kohler, Y. Iwamoto, K. Yang, B. Askevold, N. Kolishetti, M. Pittet, S. Lippard, O. Farokhzad and R. Weissleder, *Nat. Commun.*, 2015, 6, 8692.
- 30 M. Stilgenbauer, A. M. D. S. Jayawardhana, P. Datta, Z. Yue, M. Gray, F. Nielsen, D. J. Bowers, H. Xiao and Y. R. Zheng, Chem. Commun., 2019, 55, 6106–6109.
- 31 A. M. D. S. Jayawardhana and Y. R. Zheng, *Dalton Trans.*, 2022, **51**, 2012–2018.
- 32 D. Wei, Y. Yu, X. Zhang, Y. Wang, H. Chen, Y. Zhao, F. Wang, G. Rong, W. Wang, X. Kang, J. Cai, Z. Wang, J. Y. Yin, M. Hanif, Y. Sun, G. Zha, L. Li, G. Nie and H. Xiao, ACS Nano, 2020, 14, 16984–16996.

- 33 F. Zhou, B. Feng, H. Yu, D. Wang, T. Wang, Y. Ma, S. Wang and Y. Li, *Adv. Mater.*, 2019, 31, e1805888.
- 34 X. Kang, Y. Wang, Z. Chen, Y. Wu, H. Chen, X. Yang and C. Yu, *Chem. Commun.*, 2020, 56, 11271–11274.
- 35 J. Ma, Q. Wang, Z. Huang, X. Yang, Q. Nie, W. Hao, P. G. Wang and X. Wang, J. Med. Chem., 2017, 60, 5736– 5748.
- 36 A. Abu Ammar, R. Raveendran, D. Gibson, T. Nassar and S. Benita, J. Med. Chem., 2016, 59, 9035–9046.
- 37 R. Gentsch, F. Pippig, K. Nilles, P. Theato, R. Kikkeri, M. Maglinao, B. Lepenies, P. H. Seeberger and H. G. Börner, *Macromolecules*, 2010, 43, 9239–9247.
- 38 S. Bhandari, M. S. Cheung, E. Geva, L. Kronik and B. D. Dunietz, *J. Chem. Theory Comput.*, 2018, 14, 6287–6294.
- 39 S. Bhandari and B. D. Dunietz, *J. Chem. Theory Comput.*, 2019, **15**, 4305–4311.
- 40 E. Epifanovsky, A. T. B. Gilbert, X. Feng, J. Lee, Y. Mao, N. Mardirossian, P. Pokhilko, A. F. White, M. P. Coons, A. L. Dempwolff, Z. Gan, D. Hait, P. R. Horn, L. D. Jacobson, I. Kaliman, J. Kussmann, A. W. Lange, K. U. Lao, D. S. Levine, J. Liu, S. C. McKenzie, A. F. Morrison, K. D. Nanda, F. Plasser, D. R. Rehn, M. L. Vidal, Z. Q. You, Y. Zhu, B. Alam, B. J. Albrecht, A. Aldossary, E. Alguire, J. H. Andersen, V. Athavale, D. Barton, K. Begam, A. Behn, N. Bellonzi, Y. A. Bernard, E. J. Berquist, H. G. A. Burton, A. Carreras, K. Carter-Fenk, R. Chakraborty, A. D. Chien, K. D. Closser, V. Cofer-Shabica, S. Dasgupta, M. de Wergifosse, J. Deng, M. Diedenhofen, H. Do, S. Ehlert, P. T. Fang, S. Fatehi, Q. Feng, T. Friedhoff, J. Gayvert, Q. Ge, G. Gidofalvi, M. Goldey, J. Gomes, C. E. González-Espinoza, S. Gulania, A. O. Gunina, M. W. D. Hanson-Heine, P. H. P. Harbach, A. Hauser, M. F. Herbst, M. Hernández Vera, M. Hodecker, Z. C. Holden, S. Houck, X. Huang, K. Hui, B. C. Huynh, M. Ivanov, A. Jász, H. Ji, H. Jiang, B. Kaduk, S. Kähler, K. Khistyaev, J. Kim, G. Kis, P. Klunzinger, Z. Koczor-Benda, J. H. Koh, D. Kosenkov, L. Koulias, T. Kowalczyk, C. M. Krauter, K. Kue, A. Kunitsa, T. Kus, I. Ladjánszki, A. Landau, K. V. Lawler, D. Lefrancois, S. Lehtola, R. R. Li, Y. P. Li, J. Liang, M. Liebenthal, H. H. Lin, Y. S. Lin, F. Liu, K. Y. Liu, M. Loipersberger, A. Luenser, A. Manjanath, P. Manohar, E. Mansoor, S. F. Manzer, S. P. Mao, A. V. Marenich, T. Markovich, S. Mason, S. A. Maurer, P. F. McLaughlin, M. F. S. J. Menger, J. M. Mewes, S. A. Mewes, P. Morgante, J. W. Mullinax, K. J. Oosterbaan, G. Paran, A. C. Paul, S. K. Paul, F. Pavošević, Z. Pei, S. Prager, E. I. Proynov, Á. Rák, E. Ramos-Cordoba, B. Rana, A. E. Rask, A. Rettig, R. M. Richard, F. Rob, E. Rossomme, T. Scheele, M. Scheurer, M. Schneider, N. Sergueev, S. M. Sharada, W. Skomorowski, D. W. Small, C. J. Stein, Y. C. Su, E. J. Sundstrom, Z. Tao, J. Thirman, G. J. Tornai, T. Tsuchimochi, N. M. Tubman, S. P. Veccham, O. Vydrov, J. Wenzel, J. Witte, A. Yamada, K. Yao, S. Yeganeh, S. R. Yost, A. Zech, I. Y. Zhang, X. Zhang, Y. Zhang, D. Zuev, A. Aspuru-Guzik, A. T. Bell,

N. A. Besley, K. B. Bravaya, B. R. Brooks, D. Casanova, J. D. Chai, S. Coriani, C. J. Cramer, G. Cserey, A. E. DePrince, R. A. DiStasio, A. Dreuw, B. D. Dunietz, T. R. Furlani, W. A. Goddard, S. Hammes-Schiffer, T. Head-Gordon, W. J. Hehre, C. P. Hsu, T. C. Jagau, Y. Jung, A. Klamt, J. Kong, D. S. Lambrecht, W. Liang, N. J. Mayhall, C. W. McCurdy, J. B. Neaton, C. Ochsenfeld, J. A. Parkhill,

R. Peverati, V. A. Rassolov, Y. Shao, L. V. Slipchenko, T. Stauch, R. P. Steele, J. E. Subotnik, A. J. W. Thom, A. Tkatchenko, D. G. Truhlar, T. Van Voorhis, T. A. Wesolowski, K. B. Whaley, H. L. Woodcock, P. M. Zimmerman, S. Faraji, P. M. W. Gill, M. Head-Gordon, J. M. Herbert and A. I. Krylov, *J. Chem. Phys.*, 2021, 155, 084801.